NeuroImage 218 (2020) 116944

Contents lists available at ScienceDirect

NeuroImage

journal homepage: www.elsevier.com/locate/neuroimage

White matter hyperintensities are associated with subthreshold amyloid accumulation

Alexis Moscoso [a,b], David Rey-Bretal [b], Jesús Silva-Rodríguez [a,b], Jose M. Aldrey [c], Julia Cortés [a], Juan Pías-Peleteiro [c], Álvaro Ruibal [a,b], Pablo Aguiar [a,b,*], for the Alzheimer's Disease Neuroimaging Initiative[1]

[a] Nuclear Medicine Department, University Hospital CHUS-IDIS, Travesía da Choupana S/n, Santiago de Compostela, 15706, Spain
[b] Molecular Imaging Group, Department of Radiology, Faculty of Medicine, University of Santiago de Compostela (USC), Campus Vida, Santiago de Compostela, 15782, Spain
[c] Neurology Department, University Hospital CHUS-IDIS, Travesía da Choupana S/n, Santiago de Compostela, 15706, Spain

A B S T R A C T

The association between white matter hyperintensities (WMH) and amyloid accumulation over time in cognitively normal, amyloid-negative elderly people remains largely unexplored. In order to study whether baseline WMH were associated with longitudinal subthreshold amyloid accumulation, 159 cognitively normal participants from the Alzheimer's Disease Neuroimaging Initiative who were amyloid-negative at baseline were examined. All the participants underwent a T1 and a Fluid-Attenuated Inversion Recovery MRI scan at baseline. Amyloid PET imaging was performed at baseline and follow-up visits in 2-year intervals for up to 8 years. Partial volume correction was applied for quantifying cortical Standardised Uptake Value Ratios (SUVR). The associations between global and regional WMH burden and amyloid accumulation were assessed using linear mixed models adjusted by demographic characteristics and baseline SUVR. Partial volume correction increased the measured annual rate of change (+2.4%) compared to that obtained from non-corrected data (+0.5%). There were no significant correlations between baseline WMHs and baseline subthreshold cortical amyloid uptake. In a longitudinal analysis, increased baseline cortical SUVR and increased baseline burden of global (p = 0.006), frontal (p = 0.006), and parietal WMH (p = 0.003) were associated with faster amyloid accumulation. WMH-related amyloid accumulation occurred in parietal, frontal, and, to a lesser extent, cingulate cortices. These results remained unchanged after a sensitivity analysis excluding participants with the highest cortical SUVRs. This is the first study to identify a specific spatial distribution of WMH which is associated with future amyloid accumulation in cognitively normal elderly subjects without PET-detectable amyloid pathology. These findings may have important implications in prevention trials for the early identification of amyloid accumulation.

1. Introduction

White matter hyperintensities (WMH), assessed with Fluid-Attenuated Inversion Recovery (FLAIR) MRI, are common radiological findings in the aging brain (Prins and Scheltens, 2015). Although initially believed to be exclusively associated with small vessel cerebrovascular disease, an expanding body of literature suggests that the emergence of WM abnormalities is also secondary to Alzheimer's disease (AD) pathologic changes (Nasrabady et al., 2018; Araque Caballero et al., 2018; Dean et al., 2017; Strain et al., 2018; Jacobs et al., 2018). In this regard, WMH were found to be associated with tau burden and neurodegeneration in AD (McAleese et al., 2015, 2017; Tosto et al., 2015), Wallerian degeneration being the most likely mechanism for this white matter (WM) disruption (Rotshenker, 2011). However, evidence from the Dominantly Inherited Alzheimer Network (DIAN) indicates that WMH in posterior areas of the brain emerge in tandem with changes in cerebrospinal fluid (CSF) Aβ-42 and p-tau levels (Lee et al., 2016), suggesting that WMH are one of the earliest pathological features of AD and challenging the Wallerian degeneration hypothesis. These findings were supported by a recent report showing that a wide pattern of WMH, concentrated in parietal and frontal regions, was associated with PET-measured amyloid—but not tau—deposition in cognitively unimpaired elderly subjects (Graff-Radford et al., 2019). Consistent findings were also reported in a recent study using CSF-based measures of amyloid and tau deposition (Weaver et al., 2019), in which only low CSF Aβ-42 levels were associated with posterior parieto-occipital WMH.

* Corresponding author. Choupana s/n, Santiago de Compostela, 15706, Spain.
E-mail address: pablo.aguiar.fernandez@sergas.es (P. Aguiar).

[1] Data used in preparation of this article were obtained from the Alzheimer's Disease Neuroimaging Initiative (ADNI) database (adni.loni.usc.edu). As such, the investigators within the ADNI contributed to the design and implementation of ADNI and/or provided data but did not participate in the analysis or the writing of this report. A complete listing of ADNI investigators can be found at: http://adni.loni.usc.edu/wpcontent/uploads/how_to_apply/ADNI_Acknowledgement_List.pdf.

https://doi.org/10.1016/j.neuroimage.2020.116944
Received 1 April 2020; Received in revised form 30 April 2020; Accepted 11 May 2020

However, it is not clear whether amyloid-related WMH become detectable before amyloid deposition in a PET scan. If so, WMH may potentially help to identify amyloid 'accumulators' with subclinical levels of pathology, who might be optimal candidates for anti-amyloid therapies (McMillan and Chételat, 2018).

In the present study, we aimed at investigating whether measurable WMH preceded PET-detectable amyloid deposition. For this, we studied the associations between baseline global and regional patterns of WMH and amyloid accumulation over time in cognitively normal, amyloid-negative participants from the Alzheimer's Disease Neuroimaging Initiative (ADNI).

2. Methods

2.1. Study design

Data used in the preparation of this article were obtained from the ADNI database, at http://adni.loni.usc.edu. The ADNI was launched in 2003 as a public-private partnership, led by Principal Investigator Michael W. Weiner, MD. The primary goal of ADNI has been to test whether serial MRI, PET, other biological markers, and clinical and neuropsychological assessment can be combined to measure the progression of MCI and early AD. Data were downloaded from the LONI website in February 2019.

Only ADNIGO-2 participants who were cognitively normal (CN) at baseline and underwent concurrent baseline T1-weighted, FLAIR, and amyloid (Florbetapir) PET scans were considered for this study. These participants were further classified into amyloid-positive or -negative using a pre-specified cut-point for the Florbetapir PET standardised uptake value ratio (SUVR) in a cortical summary region of interest (ROI) normalised to whole cerebellum uptake (SUVR = 1.11) (Landau et al., 2013). This information was made publicly available by the ADNI PET core at http://adni.loni.usc.edu/data-samples/access-data/. For the purposes of this study, only amyloid-negative participants (SUVR < 1.11, n = 190) were included. Of the 190 participants, 159 were subjected to at least one longitudinal amyloid PET scan. Detailed information about the eligibility criteria for the different diagnostic cohorts and imaging protocols can be found at http://adni.loni.usc.edu/methods/documents/.

2.2. Informed consent

All participants provided written informed consent approved by the institutional review board of each ADNI-participating institution.

2.3. Magnetic resonance imaging acquisition and pre-processing

MRI was performed at 3 T to obtain T1-weighted and FLAIR sequences. T1 scans were pre-processed by the ADNI MRI core as previously described (Jack et al., 2011). Briefly, T1 pre-processing steps included 1) scanner-specific correction for distortions due to gradient nonlinearity (Gradwarp) (Jovicich et al., 2006); 2) application of correction for image intensity non-uniformity (B1) (Jack et al., 2008); and 3) bias field correction (N3) (Sled et al., 1998). Spatial resolution was 1 mm in the axial plane, with slice thickness of 1.2 mm. FLAIR scans were obtained with spatial resolution of 0.86 × 0.86 × 5 mm and were bias-field corrected as part of the automated pipeline for the segmentation of WMH (see below). Additional details of all MRI T1-weighted and FLAIR images can be found at http://adni.loni.usc.edu/methods/documents/mri-protocols/.

2.4. Amyloid PET acquisition and pre-processing

Florbetapir scans were performed with a dynamic protocol of four frames of 5 min acquired 50–70 min after injection. Frames were realigned, averaged, resliced to a common grid (1.5 mm^3), and smoothed to a resolution of 8 mm^3, corresponding to the lowest scanner resolution in ADNI. Follow-up amyloid PET scans were acquired at approximately 2-year intervals.

2.5. Image analysis

2.5.1. MRI processing

Pre-processed T1 images were parcellated with FreeSurfer (v6.0) to derive cortical regions of interest for PET quantification. We inspected the resulting segmentations to ensure that no gross errors occurred. No further manual corrections of the parcellations were required.

Binary WMH maps were obtained using the Lesion Segmentation Toolbox (LST) in SPM12 (Schmidt et al., 2012), using a kappa value of 0.25 and a probability threshold of 1, as previously used with ADNI data (Sudre et al., 2017). We visually inspected and manually edited the WMH maps to remove non-WM voxels labelled as WMH (manual editing was necessary in n = 25 participants) using Amide (http://amide.sourceforge.net/).

In order to measure WMH burden in brain lobes, we first filled lesions in T1 scans using the LST toolbox (Schmidt et al., 2012) to avoid incorrect segmentations of WMH as CSF or grey matter. Then, filled T1 scans were spatially normalised using SPM12 *'Normalise'* with default settings (using tpm.nii tissue priors included in SPM12). Using the inverse of this transformation, we brought back the Hammersmith atlas (Hammers et al., 2003) to patient space and merged the regions which constitute the frontal, temporal, parietal, and occipital lobes in this atlas. Since WMH maps are by default generated in co-registration with T1 images, WMH voxels lying in these lobar regions were used to compute lobar WMH volumes. The latter were normalised to total intracranial volume (TIV), as estimated with SPM12-derived segments (using SPM12 function *'Segment')* by the *'Tissue Volumes'* tool (Malone et al., 2015).

To conduct WMH voxel-wise analyses, we used the previously derived deformation field to normalise WMH maps with nearest neighbour interpolation and voxel size of 1.5 × 1.5 × 1.5 mm. Binary normalised maps were then smoothed using an isotropic 8-mm Gaussian filter and re-binarised so that only voxels with a probability >0.15 of being WMH at this resolution were labelled as WMH. This threshold was found to provide a spatial dilation to the lesions which is consistent with the spatial resolution (8 mm) we set for this analysis, while removing below-resolution clusters. Voxel-wise results remained almost unchanged when this threshold was varied over a range of 0.10–0.20.

2.5.2. Amyloid PET processing

Pre-processed Florbetapir images were co-registered to the FreeSurfer-parcellated T1 image which was closest in time, using FreeSurfer's function *mri_coreg*. Results were visually inspected to ensure correct co-registration. In four scans, manual reorientation prior to running *mri_coreg* was necessary to achieve correct registration. Co-registered images were corrected by partial volume effects (PVE) using the Symmetric Geometric Transfer Matrix (SGTM) method (Labbé et al., 1998), as implemented in PETSurfer (Greve et al., 2014). A point spread function of 8 mm was assumed for all PET images, as previously performed with ADNI data (Brendel et al., 2015). Since this study is focused on amyloid accumulation over time in amyloid-negative participants, PVE correction is essential for avoiding the confounding effect of spill-in counts from the WM, the effect of which is more severe for higher contrasts between grey and WM (López-González et al, et al; Matsubara et al, et al). Furthermore, SGTM was previously found to improve longitudinal amyloid PET measurements (Brendel et al., 2015).

PVE-corrected global amyloid burden was calculated using SUVR in the ADNI cortical summary region (Landau et al., 2013) normalised by cerebellar grey matter. Although WM reference regions have been recommended by the ADNI PET core for longitudinal Amyloid PET imaging (https://adni.bitbucket.io/reference/docs/UCBERKELEYAV45/ADNI_AV45_Methods_JagustLab_06.25.15.pdf), recent studies have shown that tracer uptake in WMH is lower than in normal-appearing WM (Zeydan et al., 2019; Glodzik et al., 2015). Since we are exploring associations

Table 1
Demographics and imaging characteristics of the study participants. Results are displayed as mean (SD) for age and baseline cortical SUVR, and as median (range) for baseline white matter hyperintensity volume. Cortical SUVR change was estimated using both fixed and random effects of a linear mixed model with time as the only fixed effect and random intercepts and slopes per subject. Abbreviations: SUVR: Standardized uptake value ratio.

	(n = 190)
Age, years	73.1 (6.3)
Females (%)	46.8
APOE ε4 carriers (%)	20.0
Baseline white matter hyperintensity volume, cm^3	
Global	1.4 (0–41.4)
Frontal	0.6 (0–28.8)
Parietal	0.12 (0–21.8)
Occipital	0.10 (0–3.3)
Temporal	0.02 (0–2.7)
Baseline cortical SUVR	0.92 (0.13)
Cortical SUVR change, SUVR/year	0.022 (0.003)
Number of participants with follow-up amyloid PET scans	
N = 0	31
N = 1	43
N = 2	66
N = 3	48
N = 4	2

between WMH and amyloid accumulation, the use of WM reference regions may result in artificially elevated cortical SUVR values and incorrect inferences. Therefore, throughout this study, only PVE-corrected data and cerebellar grey matter reference regions were used.

2.6. Statistical analysis

Cross-sectional associations between baseline, normalised WMH volumes (independent variable), and cortical SUVR (dependent variable) were assessed using linear regression, after covariate adjustment by age, sex, and APOE carriage. Linear mixed models with subject-specific intercepts and time slopes were fitted using the MATLAB function '*fitlme*' to investigate whether baseline WMH were associated with longitudinal changes in amyloid burden. The covariance matrix for random effects was fully determined using Cholesky parametrisation. We conducted these analyses for both longitudinal SUVRs in the ADNI cortical aggregate (Landau et al., 2013) as well as for each of the 19 ROIs (left- and right-averaged) which comprise this cortical aggregate. The models included age, sex, APOE status, baseline (cortical or regional) SUVR, and baseline, TIV-normalised WMH volume, as well as their interaction with continuous time. Inspection of model residuals, QQ plots, and fitted vs. residuals plots ascertained that non-linear transformation of the variables was not required. Additionally, these analyses were confirmed by studying the correlation between baseline WMH and rate of cortical SUVR annual change. For this, we fitted robust bisquare linear regressions to avoid potential effects of outliers and tested the significance of the slopes using a 5000-repetition bootstrap procedure. Annual rates of cortical SUVR change were estimated using both fixed and random effects of baseline cortical SUVR-adjusted mixed models.

In order to study the spatial WMH patterns associated with amyloid accrual, we used similar mixed models at the WMH voxel level, replacing baseline, normalised WMH volume by a binary variable indicating whether that voxel is a WMH (1) or normal-appearing WM (0) in the normalised and smoothed WMH maps (Section 2.5.1). Only voxels with WMH in at least six participants (minimum number required to determine model coefficients) and with a probability of being WM > 0.90 (according to the WM SPM12 tissue probability map in MNI space) were considered for the analysis.

A False Discovery Rate (FDR) (Genovese et al., 2002) correction of $\alpha = 0.05$ was used to correct both the ROI and voxel-based analyses for multiple comparisons. For sensitivity analysis, key findings were replicated using a more restrictive cut-point for amyloid negativity (5% lower, PVE-uncorrected SUVR = 1.05, n = 120 participants for the longitudinal analysis). All the analyses were carried out in MATLAB 2017a.

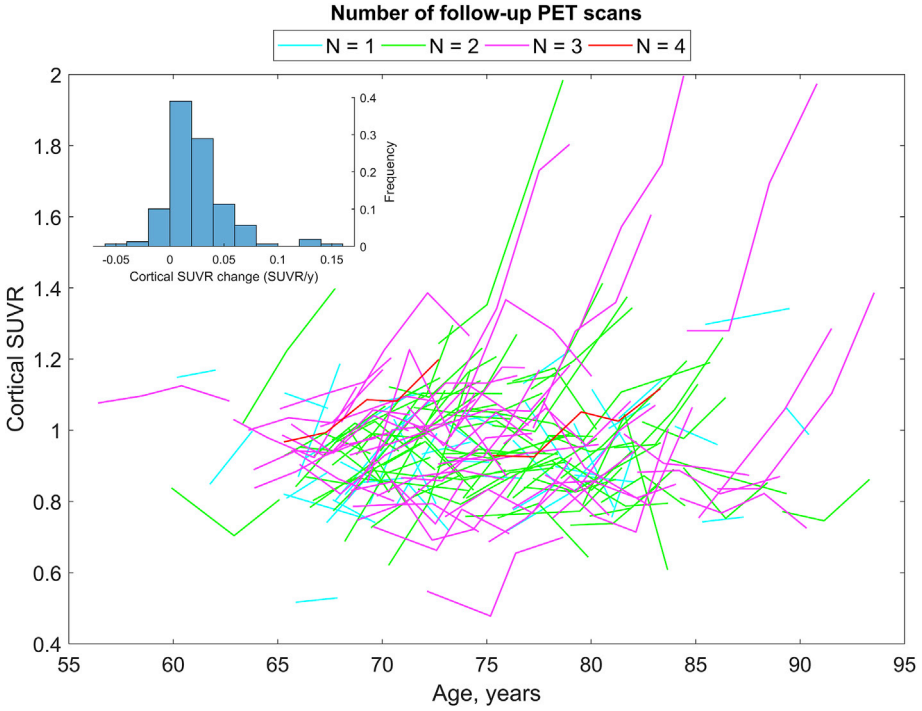

Fig. 1. Longitudinal trajectories of amyloid accumulation, as a function of age. The different colours are used to represent the number of follow-up amyloid PET scans. The embedded histogram represents annual rates of cortical SUVR change, as estimated using both fixed and random effects of a linear mixed model with time as the only fixed effect and random intercepts and slopes per subject. Abbreviations: SUVR: Standardized Uptake Value Ratio.

Table 2
Linear mixed model results for the association between baseline WMH normalised volumes and amyloid accumulation over time. Results are expressed as standardized β′s of the time interaction coefficient of WMH and baseline SUVR. Model 1 included only adjustment by baseline cortical SUVR (SUVR ~ time*(baseline_SUVR + WMH) + (time|rid) in Wilkinson notation), while Model 2[a] included age, sex, and APOE as well (SUVR ~ time*(baseline_SUVR + WMH + age + sex + APOE) + (time|rid)). Model 2[b] was the same as 2[a] but was fitted in the subset of participants who were amyloid negative with the more restrictive cut-point of PVE uncorrected SUVR = 1.05, in order to perform a sensitivity analysis. No significant covariate × time terms were found in Models 2[a] and 2[b]. Abbreviations: WMH: White matter hyperintensities; SUVR: Standardized uptake value ratio.

WMH predictor	Model 1		Model 2[a]		Model 2[b]	
	β (95% CI)	*p* value	β (95% CI)	*p* value	β (95% CI)	*p* value
Global						
Global WMH × time	0.19 (0.09 to 0.29)	<0.001	0.15 (0.04 to 0.26)	0.006	0.19 (0.09 to 0.28)	<0.001
Baseline SUVR × time	0.10 (0.04 to 0.16)	0.002	0.12 (0.05 to 0.18)	<0.001	0.03 (−0.04 to 0.10)	0.40
Frontal						
Frontal WMH × time	0.17 (0.08 to 0.26)	<0.001	0.13 (0.04 to 0.23)	0.006	0.14 (0.05 to 0.22)	0.001
Baseline SUVR × time	0.11 (0.05 to 0.17)	<0.001	0.12 (0.06 to 0.19)	<0.001	0.03 (−0.05 to 0.10)	0.48
Parietal						
Parietal WMH × time	0.23 (0.10 to 0.37)	<0.001	0.20 (0.07 to 0.33)	0.003	0.24 (0.10 to 0.37)	<0.001
Baseline SUVR × time	0.08 (0.02 to 0.14)	0.01	0.11 (0.04 to 0.17)	0.001	0.03 (−0.04 to 0.10)	0.40
Occipital						
Occipital WMH × time	0.03 (−0.06 to 0.11)	0.54	−0.004 (−0.08 to 0.07)	0.92	0.01(-0.07 to 0.09)	0.78
Baseline SUVR × time	0.10 (0.03 to 0.17)	0.003	0.12 (0.06 to 0.19)	<0.001	0.04 (−0.04 to 0.11)	0.36
Temporal						
Temporal WMH × time	0.008 (−0.09 to 0.10)	0.88	−0.03 (−0.13 to 0.06)	0.49	0.08 (−0.05 to 0.22)	0.21
Baseline SUVR × time	0.10 (0.03 to 0.17)	0.003	0.13 (0.06 to 0.19)	<0.001	0.04 (−0.04 to 0.11)	0.32

2.7. Data and code availability statement

Data used in the preparation of this article were obtained from the publicly available ADNI database, at http://adni.loni.usc.edu. All the code used in this manuscript has been written in MatLab and will be provided to investigators upon request.

3. Results

3.1. Cohort characteristics

Demographic characteristics of the subjects included in this study are presented in Table 1. Of the study subjects, 159 participants had at least one follow-up amyloid PET scan. Median amyloid PET follow-up was 4.4 years, with a range from 1 to 8 years. The rate of cortical SUVR annual change, estimated as the fixed effect of a mixed model with time as the only fixed effect, was higher with PVE correction (0.022, 95% CI: 0.016 to 0.028, 2.4% when compared to PVE-corrected, mean baseline cortical SUVR) than without (0.006, 95% CI: 0.003 to 0.009, 0.5% when compared to PVE-uncorrected, mean baseline cortical SUVR). Accumulation trajectories are depicted in Fig. 1 At follow-up, 21 subjects were converted to amyloid-positive, as determined by the PVE-uncorrected cut-point provided by ADNI (SUVR = 1.11).

3.2. Baseline WMH are associated with amyloid accumulation

First, we studied the cross-sectional association between baseline cortical SUVR and baseline normalised WMHs by running separate linear regressions for both global and each regional WMH, adjusting by age, sex, and APOE. Although all the WMH coefficients were positively associated with baseline cortical SUVR, none reached statistical significance (global WMH: $\beta = 0.13$, $p = 0.08$; frontal WMH: $\beta = 0.24$, $p = 0.07$; parietal WMH: $\beta = 0.23$, $p = 0.23$; temporal WMH: $\beta = 0.92$, $p = 0.44$; occipital WMH: $\beta = 0.69$, $p = 0.47$). Males presented with higher cortical SUVR ($\beta = 0.62$, $p < 0.001$ in a model with age, sex, and APOE as the only predictors).

In longitudinal analysis, we assessed whether WMHs were associated with amyloid accumulation over time. The results of the mixed models are summarised in Table 2. Apart from the significant effect of baseline cortical SUVR, higher global, frontal, and parietal WMH burden was significantly associated with faster rates of global amyloid accumulation, with and without adjustment by demographic covariates (Table 2, Model 1 and 2[a]). These significant relationships can be further visualised in Fig. 2. After repeating the adjusted analysis with a more restrictive cut-point (n = 120, with uncorrected cortical SUVRs normalised to cerebellum < 1.05), the association with baseline cortical SUVR disappeared but the association with WMH remained almost unchanged (Table 2, Model 2[b]).

3.3. Spatial patterns of WMH associated with amyloid accumulation

Here, we aimed at focusing more specifically on the WMH spatial patterns related to amyloid accumulation. We utilised linear mixed models at the WMH voxel level, as detailed in Sections 2.5.1 and 2.6, adjusted by age, sex, and APOE. Fig. 3A and B depicts both the frequency of WMH lesions and the spatial pattern of WMH associated with amyloid accumulation, respectively. These WMH clusters spanned parietal and frontal lobes, confirming the analyses at the ROI level. Compared to the areas of maximum WMH frequency (Fig. 3A), amyloid accumulation related-WMH displayed a pattern of more superior accumulation in frontal and parietal lobes (Fig. 3B, top row).

3.4. Regional distribution of WMH-related amyloid accumulation

We further explored which cortical areas within the ADNI cortical aggregate (Landau et al., 2013) drove the previously observed faster accumulation. For this, we fit separate linear mixed models with each regional SUVR (response variable) and with each of those previously discovered, significant regional WMH (global, frontal, and parietal; independent variable), adjusted by baseline regional SUVR and demographics, as described in Section 2.6. Fig. 4 depicts the cortical areas in which a faster accumulation was significantly associated with higher WMH burden. As can be seen in Fig. 4A and C, global and parietal WMH displayed a similar pattern of accumulation, involving mainly frontal, parietal, and, to a lesser extent, cingulate areas. Fewer regions survived multiple comparison correction for frontal WMH, which also involve frontal, parietal, and cingulate regions (Fig. 4B). Fig. 5 illustrates the effect size of each WMH predictor on each cortical ROI.

4. Discussion

The present study investigated whether WM abnormalities, assessed as WMH with FLAIR MRI, were associated with faster rates of amyloid accumulation, as measured with amyloid PET, in cognitively normal, amyloid-negative elderly subjects. Although we did not uncover cross-sectional associations between subthreshold amyloid and WMH, our

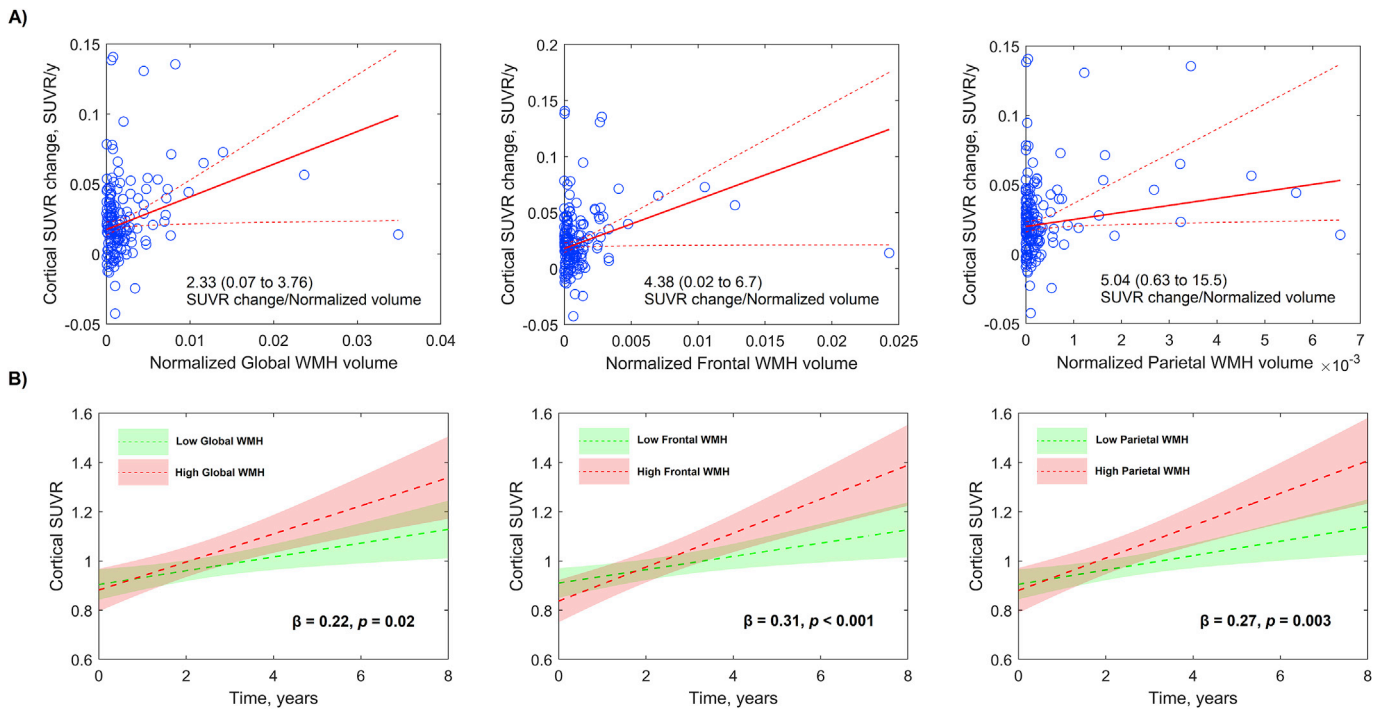

Fig. 2. A) Relationship between change in cortical SUVR and baseline WMH. Change in cortical SUVR was estimated using both fixed and random effects of a linear mixed model with time and baseline SUVR as fixed effects, and random intercepts and slopes per subject. Solid red lines represent robust bisquare linear regression fits; dashed lines represent 95% CI derived using a 5000-iteration bootstrap procedure. 95% CI for the slopes of these fits were computed using the same procedure. B) Modelled amyloid accumulation trajectories over time for subjects with high and low WMH burden. High (Low) WMH burden participants were defined as those above (below) the 85th percentile normalised WMH volume. Trajectories were estimated with linear mixed models adjusted by age, sex, APOE, and baseline SUVR, evaluated for a 75-year-old male without APOE ε4 allele and at mean covariate values.

findings suggest that a characteristic spatial pattern of WMH, spanning superior areas of the frontal and parietal lobes, is associated with future amyloid accrual, independently of continuous levels of subthreshold cortical pathology. This accumulation occurred in cortical regions previously identified as regions of early accumulation in AD (Palmqvist et al., 2017; Villeneuve et al., 2015; Mattsson et al., 2019), suggesting that the observed faster accumulation may be driven by processes related to early AD pathology. To the best of our knowledge, this is the first study in which an imaging biomarker is found to be associated with amyloid accumulation in amyloid-negative, cognitively normal individuals.

Our findings are consistent with prior cross-sectional reports simultaneously analysing the role of amyloid and tau in the emergence of WMH. The tau-independent relationship between WMH and amyloid, particularly with parietal WMH, was detected in cross-sectional studies of asymptomatic familial AD (Lee et al., 2016) and in two recent reports in cognitively unimpaired elderly subjects (Graff-Radford et al., 2019; Weaver et al., 2019). Here, we add to these previous findings by observing that a similar pattern of WMH is detectable at subclinical levels of amyloid pathology, partially supporting the hypothesis that WMH are secondary to amyloid deposition. Although the link between early amyloid deposition and WM damage is still not clear, several potential mechanisms, such as oligodendrocyte dysfunction and demyelination induced by amyloid oligomers (Nasrabady et al., 2018; Collins-Praino et al., 2014), as well as axonal degeneration secondary to amyloid-related microglia activation (Liddelow et al., 2017; Suárez-Calvet et al., 2016), might explain this relationship. However, the findings of the present study do not exclude the possibility that the observed WMH patterns had a vascular disease aetiology, with a causal or interactive link between cerebrovascular pathology and amyloid deposition, as suggested by a previous study (Hughes et al., 2018). Endothelial dysfunction or a broader blood-brain barrier dysfunction may be the key links, as they may lead to both WMH and impaired brain-blood amyloid clearance, thus favouring brain amyloid accumulation (Yamazaki and Kanekiyo, 2017; Tarantini et al., 2017; Koizumi et al., 2016). This hypothesis is also supported by the observed amyloid-related WMH spatial pattern, which is similar to the pattern of WMH associated to cerebrovascular disease (Al-Janabi et al., 2018). It must be noted that this mechanism also implies that the observed increase in WMH burden with familial AD progression (Lee et al., 2016) may be a specific feature of familial AD and not of sporadic AD. More neuropathological and imaging studies are warranted to understand fully the relationship between early amyloid accumulation, WM disease, and vascular pathology.

At the regional level, the observed topographic pattern is congruent with patterns observed in previous studies analysing the relationship between amyloid and WMH in elderly subjects (Graff-Radford et al., 2019; Weaver et al., 2019; Al-Janabi et al., 2018). Of note, patterns found in CSF studies (Weaver et al., 2019; Al-Janabi et al., 2018) spanned only posterior parieto-occipital regions while our findings and those from a recent cross-sectional PET study (Graff-Radford et al., 2019) cover both posterior and frontal regions. The fact that CSF studies failed in detecting associations of frontal WMH with amyloid pathology can be explained by a number of reasons such as differences in statistical power or the fact that CSF Aβ-42 levels are sensitive to other pathologies, including WM damage (Skoog et al., 2018). Given that the WMH pattern associated with vascular disease covers frontal regions (Al-Janabi et al., 2018), an even higher confounding effect in these areas can be expected in CSF studies. In familial AD, frontal and posterior WMH seem to emerge earlier in the disease course (Lee et al., 2016), in line with findings from a neuroimaging study which suggests that spatial patterns of amyloid-related WMH are different from those of vascular aetiology (Al-Janabi et al., 2018) and strengthening the amyloidogenic hypothesis for WMH. Taken together, all these findings converge in identifying posterior WMH as related to amyloid plaque deposition. Although we and others (Graff-Radford et al., 2019) have shown that also frontal WMH associate with amyloid deposition, the fact that WMH of vascular aetiology concentrate in both frontal and posterior regions (Al-Janabi et al., 2018) suggests that

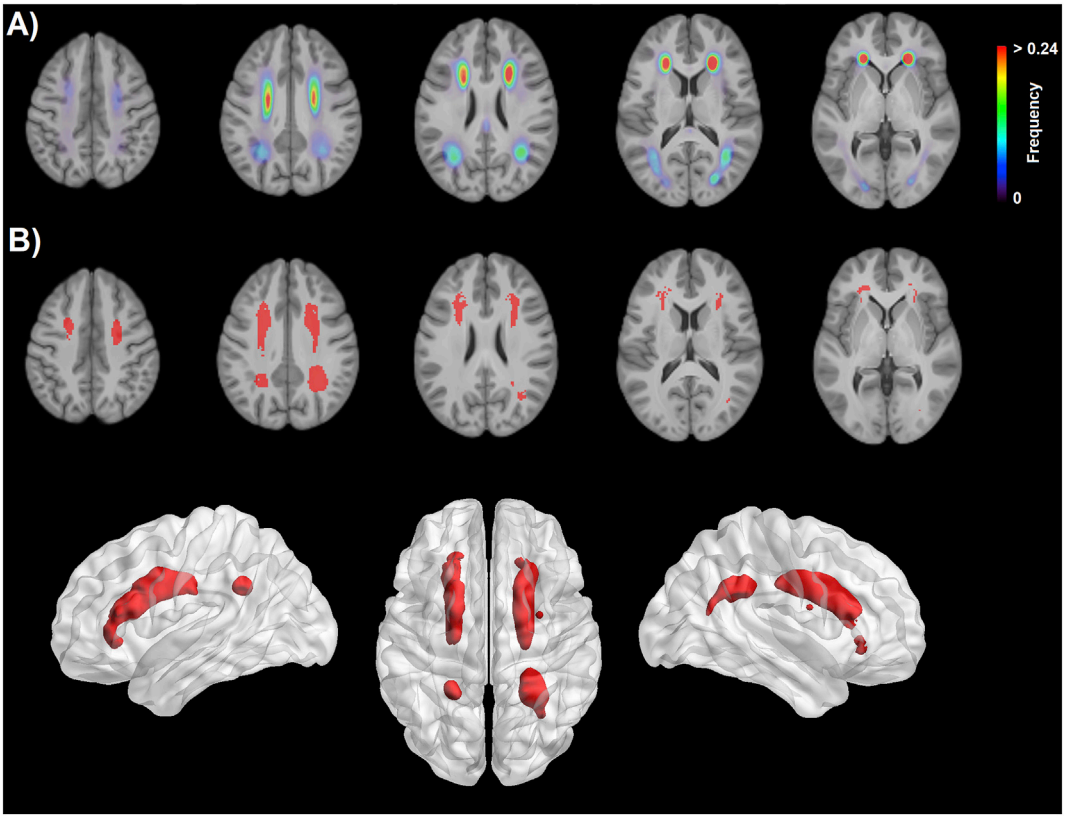

Fig. 3. A) Spatial frequency of WMH among the study participants. B) Top row: Spatial distribution of WMH (in red) associated with faster amyloid accumulation, for the same axial slices as on top row. Bottom Row: 3D rendering of the spatial WMH pattern (in red) of middle row. WMH maps associated with amyloid accumulation were obtained using linear mixed models at the WMH-voxel level. Because for a significant proportion of voxels data was not enough to estimate random slopes, the model included only random intercepts per subject. Anatomical left/right is on the left/right of the image. Frequency represents the proportion (0–1) of subjects with WMH.

the assessment of WMH in posterior regions might be the optimal measure for the potential identification of early amyloid pathology.

From a mechanistic point of view, it is still unclear why certain WM regions might be more vulnerable to amyloid-related WMH. Unfortunately, in the absence of a feasible theoretical mechanism, correlational studies cannot conclude whether the differences in patterns are due to biological mechanisms or simply due to confounding effects resulting from overlapping vascular pathology in the elderly. Further investigation is warranted to understand fully whether the relationship between amyloid and the WM is global or region-specific.

We also observed that the dependence of the rate of amyloid accumulation and WMH seems to follow an inverted U-shape. Again, it is difficult to hypothesize on the origin of this behaviour without a clear biological mechanism. A potential reason might be the presence of increased WMH burden due to non-AD pathologies; however, little is known about amyloid accumulation in the subthreshold regime, and more complex accumulation trajectories might exist. Further studies are needed to understand the biological mechanisms behind these findings.

The relationship between amyloid and WMH burden in preclinical AD has been explored before but findings were often conflicting. Apart from the three large studies mentioned above that controlled for the influence of tau (Graff-Radford et al., 2019; Weaver et al., 2019), other previous smaller studies have investigated how WMH relate to amyloid using both amyloid PET and CSF. Apparently, the rate of positive findings is significantly higher in CSF studies than when using amyloid PET. According to a review paper (Roseborough et al., 2017), only 2 out of 13 studies reported a positive correlation between amyloid and WMH burden, in contrast to the multiple CSF studies which found a positive association (see, for instance (Kandel et al., 2016; Marnane et al., 2016; Pietroboni et al., 2018; Scott et al., 2016; Scott et al., 2015),). Potential explanations include the non-regional assessment of WMH, small sample sizes, the higher sensitivity of CSF for early amyloid pathology (Palmqvist et al., 2016), and the fact that, as we have shown, amyloid-related WMH might be elevated at subthreshold levels. In this regard, our results also emphasize the need to redefine current amyloid PET cut-points to capture early amyloid pathology, as other studies have pointed out (Villeneuve et al., 2015).

Apart from WMH measured with FLAIR, other studies using diffusion tensor imaging (DTI) in WM reported changes associated with amyloid burden at different DTI metrics (Molinuevo et al., 2014). As with WMH, results are conflicting (Molinuevo et al., 2014; Racine et al., 2014), probably for the reasons previously discussed. Particularly interesting is a study in which a DTI measure of myelin was found to be associated with levels of CSF Aβ-42 (Dean et al., 2017), supporting the hypothesis of amyloid-related oligodendrocyte dysfunction. Future studies will assess how white matter integrity and myelin relates to longitudinal amyloid accumulation in amyloid-negative elderly subjects.

The fact that a regional distribution of WMH might be predictive of amyloid deposition in amyloid-negative elderly has important implications for anti-amyloid clinical trials, since the majority of efforts shift now towards the prevention of amyloid pathology, even in subjects on the AD pathway but with very mild amyloid burden, the so-called amyloid 'accumulators' (McMillan and Chételat, 2018). Recent evidence suggests that 'accumulators' experience faster rates of cognitive decline (Landau et al., 2018; Farrell et al., 2018) and disrupted brain connectivity (Palmqvist et al., 2017), highlighting the clinical relevance of early amyloid accumulation. Beyond the scope of this study is the relative importance of WMH and amyloid accumulation in cognitive decline in these subjects, which may be informative for the identification of novel therapeutic targets on WM. Further studies with longer follow-up times

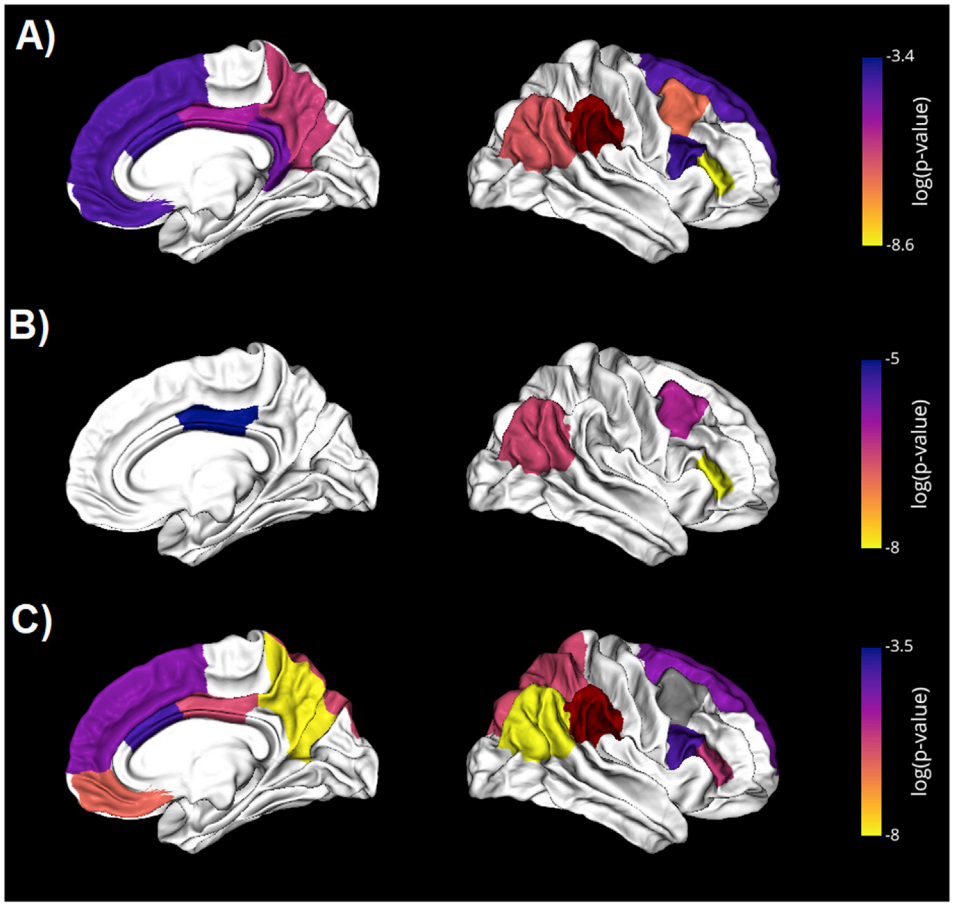

Fig. 4. Cortical regions in which amyloid accumulation is significantly (after FDR correction) associated to higher A) global WMH, B) frontal WMH, and C) parietal WMH. Linear mixed models with regional cortical SUVR as response variable, adjusted by demographics and baseline SUVR, were used. *p*-values (uncorrected) are expressed as natural log(p-value). Regions: A) Pars Triangularis, Caudal Middle Frontal, Inferior Parietal, Precuneus, Posterior Cingulate, Isthmus Cingulate, Superior Frontal, Medial Orbitofrontal, Caudal Anterior Cingulate, Pars Opercularis, Supramarginal. B) Pars Triangularis, Inferior Parietal, Caudal Middle Frontal, Posterior Cingulate. C) Caudal Middle Frontal, Inferior Parietal, Precuneus, Medial Orbitofrontal, Posterior Cingulate, Superior Parietal, Pars Triangularis, Superior Frontal, Pars Opercularis, Caudal Anterior Cingulate, Supramarginal.

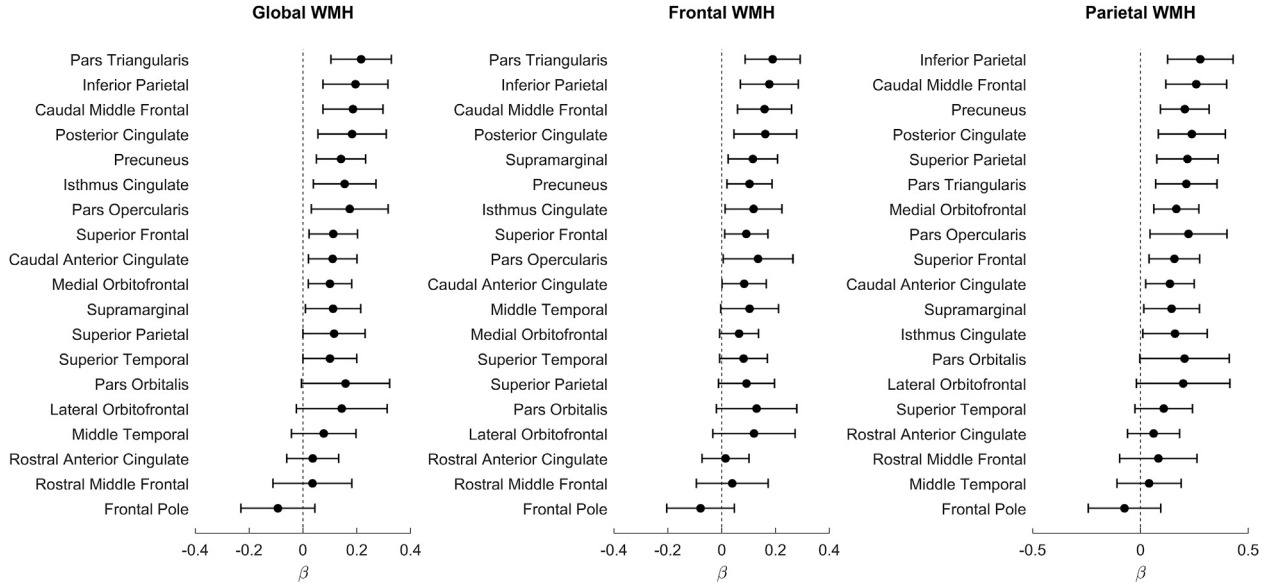

Fig. 5. Effect size (standardized β) of each WMH predictor on each of the 19 regions comprising the cortical aggregate used in this study. Standardized β′s represent the number of SD that vary in the SUVR of each region of interest with 1 SD variation in WMH, per year. Abbreviations: WMH: White matter hyperintensities.

are needed to assess how useful these WMH patterns are for identifying 'accumulators' and for predicting clinically relevant outcomes.

Remarkably, we found that males displayed higher levels of subthreshold amyloid pathology. Amyloid-related tau pathology has been found to be higher in females (Buckley et al., 2019); however, to the best of our knowledge, neither differences in amyloid burden, particularly in the subthreshold regime, nor potential biological mechanisms have been reported before. In this regard, our findings might motivate future research and generate novel hypotheses on this topic.

This study has several strengths. First, our cohort of cognitively

normal, amyloid-negative elderly subjects was relatively large. A second strength is the number of repeated amyloid PET scans, with most of the participants having two or more follow-up scans, and the length of the follow-up, with a median time of 4.4 years and longitudinal examinations of up to 8 years. A third strength is the use of partial volume correction, which improved the sensitivity for detecting changes without the use of WM reference regions, the uptake of which varies with WM pathology (Zeydan et al., 2019; Glodzik et al., 2015). This work also has certain limitations: First, the ADNI inclusion criteria only allow for participants relatively free of cerebrovascular pathology and, therefore, of WMH burden, which might compromise the generalisability of our findings in a community cohort. However, similar WMH patterns to those found in this study were found in the community cohort of the Mayo Clinic Study of Aging (Graff-Radford et al., 2019), suggesting that, despite confounding pathology, the patterns may be detectable. Second, we could not assess how the longitudinal changes in WMH relate to amyloid accumulation, since the FLAIR protocol changed at the end of ADNI2, from 2D axial FLAIR to high-resolution 3D FLAIR. Without a harmonisation method, mixing these two protocols, particularly in a longitudinal study, may lead to incorrect inferences. Third, the number of subjects with WMH in a given voxel is variable and, thus, the statistical power of voxel-wise analyses varies across the different brain regions. Although the absence of evidence can never be considered evidence of absence (Altman and Bland, 1995), this is particularly true for any voxel-wise analyses, and, therefore, other regions may also emerge as significantly associated with amyloid accumulation in more powered studies. Fourth, the pre-specified cut-point we used to select amyloid-negative participants was derived without PVE correction and may have been too high (Villeneuve et al., 2015), which may have led to a significant number of false amyloid-negative individuals. However, the sensitivity analyses we conducted and the adjustment by baseline uptake levels suggests that our findings are robust against these limitations. Fifth, WMH are a non-specific brain imaging finding and are shared by patient groups with heterogeneous aetiologies. Our findings may partially agree with those of WMH related to cerebral amyloid angiopathy (CAA), which has been shown to closely overlap AD pathology, even in the absence of conventional vascular risk factors, as observed in patients with AD and cerebral amyloid angiopathy in the context of Down syndrome (Carmona-Iragui et al., 2019). Nevertheless, three previous studies have shown that the relationship between amyloid burden and WMH is not driven by CAA (Lee et al., 2016; Graff-Radford et al., 2019; Weaver et al., 2019). Moreover, the prevalence of CAA among non-demented individuals, as detected by the presence of two or more lobar cerebral microbleeds, is ~4% (Graff-Radford et al., 2019). We thus expect an even lower prevalence in our cohort, since our participants were preselected to be relatively free of vascular pathology and were cognitively normal and amyloid-negative, making CAA an unlikely confounder.

In conclusion, we have provided further evidence supporting WMH as one of the earliest pathological features in AD progression. A specific spatial pattern of WMH has been found to be associated with future amyloid accumulation in cognitively normal older individuals with no evidence of amyloid pathology in amyloid PET. The spatial assessment of WMH may potentially allow the identification of subjects on the AD pathway with amyloid burden levels below PET detectability limits.

Declaration of competing interest

AM, DR, JS, JMA, JC, JP, AR, and PA report no relevant conflicts of interest.

CRediT authorship contribution statement

Alexis Moscoso: Writing - original draft, Formal analysis. **David Rey-Bretal:** Formal analysis. **Jesús Silva-Rodríguez:** Formal analysis. **Jose M. Aldrey:** Writing - original draft, Conceptualization. **Julia Cortés:** Writing - original draft. **Juan Pías-Peleteiro:** Writing - original draft. **Álvaro Ruibal:** Writing - review & editing. **Pablo Aguiar:** Writing - original draft, Formal analysis, Conceptualization.

Acknowledgements

Data collection and sharing for this project was funded by the Alzheimer's Disease Neuroimaging Initiative (ADNI) (National Institutes of Health Grant U01 AG024904) and DOD ADNI (Department of Defense award number W81XWH-12-2-0012). ADNI is funded by the National Institute on Aging, the National Institute of Biomedical Imaging and Bioengineering, and through generous contributions from the following: AbbVie, Alzheimer's Association; Alzheimer's Drug Discovery Foundation; Araclon Biotech; BioClinica, Inc.; Biogen; Bristol-Myers Squibb Company; CereSpir, Inc.; Cogstate; Eisai Inc.; Elan Pharmaceuticals, Inc.; Eli Lilly and Company; EuroImmun; F. Hoffmann-La Roche Ltd and its affiliated company Genentech, Inc.; Fujirebio; GE Healthcare; IXICO Ltd.; Janssen Alzheimer Immunotherapy Research & Development, LLC.; Johnson & Johnson Pharmaceutical Research & Development LLC.; Lumosity; Lundbeck; Merck & Co., Inc.; Meso Scale Diagnostics, LLC.; NeuroRx Research; Neurotrack Technologies; Novartis Pharmaceuticals Corporation; Pfizer Inc.; Piramal Imaging; Servier; Takeda Pharmaceutical Company; and Transition Therapeutics. The Canadian Institutes of Health Research is providing funds to support ADNI clinical sites in Canada. Private sector contributions are facilitated by the Foundation for the National Institutes of Health (www.fnih.org). The grantee organization is the Northern California Institute for Research and Education, and the study is coordinated by the Alzheimer's Therapeutic Research Institute at the University of Southern California. ADNI data are disseminated by the Laboratory for Neuro Imaging at the University of Southern California. This work was partially supported by the project PI16/01416 (ISCIII co-funded FEDER), EAPA_791/2018-NEUROATLANTIC, and RYC-2015/17430 (Ramón y Cajal, Pablo Aguiar).

References

Al-Janabi, O.M., Brown, C.A., Bahrani, A.A., Abner, E.L., et al., 2018. Distinct white matter changes associated with cerebrospinal fluid amyloid-β1-42 and hypertension. J Alzheimers Dis 66 (3), 1095–1104.

Altman, D.G., Bland, J.M., 1995 Aug 19. Absence of evidence is not evidence of absence. BMJ 311, 7003):485.

Araque Caballero, M.Á., Suárez-Calvet, M., Duering, M., Franzmeier, N., et al., 2018 Oct 1. White matter diffusion alterations precede symptom onset in autosomal dominant Alzheimer's disease. Brain 141 (10), 3065–3080.

Brendel, M., Högenauer, M., Delker, A., Sauerbeck, J., et al., 2015 Mar. Improved longitudinal [(18)F]-AV45 amyloid PET by white matter reference and VOI-based partial volume effect correction. Neuroimage 108, 450–459.

Buckley, R.F., Mormino, E.C., Rabin, J.S., Hohman, T.J., et al., 2019 May 1. Sex differences in the association of global amyloid and regional tau deposition measured by positron emission tomography in clinically normal older adults. JAMA Neurol 76 (5), 542–551.

Carmona-Iragui, M., Videla, L., Lleó, A., Fortea, J., 2019 Jul. Down syndrome, Alzheimer disease, and cerebral amyloid angiopathy: the complex triangle of brain amyloidosis. Dev Neurobiol 79 (7), 716–737.

Collins-Praino, L.E., Francis, Y.I., Griffith, E.Y., Wiegman, A.F., et al., 2014 Aug 17. Soluble amyloid beta levels are elevated in the white matter of Alzheimer's patients, independent of cortical plaque severity. Acta Neuropathol Commun 2, 83.

Dean 3rd, D.C., Hurley, S.A., Kecskemeti, S.R., O'Grady, J.P., et al., 2017 Jan 1. Association of amyloid pathology with myelin alteration in preclinical alzheimer disease. JAMA Neurol 74 (1), 41–49.

Farrell, M.E., Chen, X., Rundle, M.M., Chan, M.Y., et al., 2018 Nov 6. Regional amyloid accumulation and cognitive decline in initially amyloid-negative adults. Neurology 91 (19), e1809–e1821.

Genovese, C.R., Lazar, N.A., Nichols, T., 2002 Apr. Thresholding of statistical maps in functional neuroimaging using the false discovery rate. Neuroimage 15 (4), 870–878.

Glodzik, L., Rusinek, H., Li, J., Zhou, C., et al., 2015 Jan. Reduced retention of Pittsburgh compound B in white matter lesions. Eur. J. Nucl. Med. Mol. Imag. 42 (1), 97–102.

Graff-Radford, J., Arenaza-Urquijo, E.M., Knopman, D.S., Schwarz, C.G., et al., 2019 Aug 1. White matter hyperintensities: relationship to amyloid and tau burden. Brain 142 (8), 2483–2491.

Greve, D.N., Svarer, C., Fisher, P.M., Feng, L., et al., 2014 May 15. Cortical surface-based analysis reduces bias and variance in kinetic modeling of brain PET data. Neuroimage 92, 225–236.

Hammers, A., Allom, R., Koepp, M.J., Free, S.L., et al., 2003 Aug. Three-dimensional maximum probability atlas of the human brain, with particular reference to the temporal lobe. Hum. Brain Mapp. 19 (4), 224–247.
Hughes, T.M., Wagenknecht, L.E., Craft, S., Mintz, A., et al., 2018 Apr 3. Arterial stiffness and dementia pathology: atherosclerosis risk in communities (ARIC)-PET study. Neurology 90 (14), e1248–e1256.
Jack Jr., C.R., Bernstein, M.A., Fox, N.C., Thompson, P., et al., 2008. The Alzheimer's disease neuroimaging initiative (ADNI): MRI methods. J. Magn. Reson. Imag. 27, 685–691.
Jack Jr., C.R., Vemuri, P., Wiste, H.J., Weigand, S.D., et al., 2011 Dec. Evidence for ordering of Alzheimer disease biomarkers. Arch. Neurol. 68 (12), 1526–1535.
Jacobs, H.I.L., Hedden, T., Schultz, A.P., Sepulcre, J., et al., 2018 Mar. Structural tract alterations predict downstream tau accumulation in amyloid-positive older individuals. Nat. Neurosci. 21 (3), 424–431.
Jovicich, J., Czanner, S., Greve, D., Haley, E., et al., 2006. Reliability in multi-site structural MRI studies: effects of gradient non-linearity correction on phantom and human data. Neuroimage 30, 436–443.
Kandel, B.M., Avants, B.B., Gee, J.C., McMillan, C.T., et al., 2016 Apr 7. White matter hyperintensities are more highly associated with preclinical Alzheimer's disease than imaging and cognitive markers of neurodegeneration. Alzheimers Dement (Amst). 4, 18–27.
Koizumi, K., Wang, G., Park, L., 2016 Mar. Endothelial dysfunction and amyloid-β-induced neurovascular alterations. Cell. Mol. Neurobiol. 36 (2), 155–165.
Labbé, C., Koepp, M., Ashburner, J., Spinks, T., et al., 1998. Absolute PET quantification with correction for partial volume effects with cerebral structures. Quantitative Functional Brain Imagaing with Positron Emission Tomography 59–66.
Landau, S.M., Breault, C., Joshi, A.D., Pontecorvo, M., et al., 2013 Jan. Amyloid-β imaging with Pittsburgh compound B and florbetapir: comparing radiotracers and quantification methods. J. Nucl. Med. 54 (1), 70–77.
Landau, S.M., Horng, A., Jagust, W.J., 2018 Apr 24. Memory decline accompanies subthreshold amyloid accumulation. Neurology 90 (17), e1452–e1460.
Lee, S., Viqar, F., Zimmerman, M.E., Narkhede, A., et al., 2016 Jun. White matter hyperintensities are a core feature of Alzheimer's disease: evidence from the dominantly inherited Alzheimer network. Ann. Neurol. 79 (6), 929–939.
Liddelow, S.A., Guttenplan, K.A., Clarke, L.E., Bennett, F.C., et al., 2017 Jan 26. Neurotoxic reactive astrocytes are induced by activated microglia. Nature 541 (7638), 481–487.
López-González FJ, Moscoso A, Efthimiou N, Fernández-Ferreiro A, et al. Spill-in counts in the quantification of 18F-florbetapir on Aβ-negative subjects: the effect of including white matter in the reference region. EJNMMI Physics. (in press).
Malone, I.B., Leung, K.K., Clegg, S., Barnes, J., et al., 2015 Jan 1. Accurate automatic estimation of total intracranial volume: a nuisance variable with less nuisance. Neuroimage 104, 366–372.
Marnane, M., Al-Jawadi, O.O., Mortazavi, S., Pogorzelec, K.J., et al., 2016 Feb 9. Periventricular hyperintensities are associated with elevated cerebral amyloid. Neurology 86 (6), 535–543.
Matsubara K, Ibaraki M, Shimada H, Ikoma Y, et al. Impact of Spillover from White Matter by Partial Volume Effect on Quantification of Amyloid Deposition with [11C]PiB PET.
Mattsson, N., Palmqvist, S., Stomrud, E., Vogel, J., et al., 2019 Jul 17. Staging β-amyloid pathology with amyloid positron emission tomography. JAMA Neurol.
McAleese, K.E., Firbank, M., Dey, M., Colloby, S.J., et al., 2015 Sep 30. Cortical tau load is associated with white matter hyperintensities. Acta Neuropathol Commun 3, 60.
McAleese, K.E., Walker, L., Graham, S., Moya, E.L.J., et al., 2017 Sep. Parietal white matter lesions in Alzheimer's disease are associated with cortical neurodegenerative pathology, but not with small vessel disease. Acta Neuropathol. 134 (3), 459–473.
McMillan, C.T., Chételat, G., 2018 Apr 24. Amyloid "accumulators": the next generation of candidates for amyloid-targeted clinical trials? Neurology 90 (17), 759–760.
Molinuevo, J.L., Ripolles, P., Simó, M., Lladó, A., et al., 2014 Dec. White matter changes in preclinical Alzheimer's disease: a magnetic resonance imaging-diffusion tensor imaging study on cognitively normal older people with positive amyloid β protein 42 levels. Neurobiol. Aging 35 (12), 2671–2680.
Nasrabady, S.E., Rizvi, B., Goldman, J.E., Brickman, A.M., 2018 Mar 2. White matter changes in Alzheimer's disease: a focus on myelin and oligodendrocytes. Acta Neuropathol Commun 6 (1), 22.
Palmqvist, S., Mattsson, N., Hansson, O., 2016 Apr. Cerebrospinal fluid analysis detects cerebral amyloid-β accumulation earlier than positron emission tomography. Brain 139 (Pt 4), 1226–1236.
Palmqvist, S., Schöll, M., Strandberg, O., Mattsson, N., et al., 2017 Oct 31. Earliest accumulation of β-amyloid occurs within the default-mode network and concurrently affects brain connectivity. Nat. Commun. 8 (1), 1214.
Pietroboni, A.M., Scarioni, M., Carandini, T., Basilico, P., et al., 2018 Apr. CSF β-amyloid and white matter damage: a new perspective on Alzheimer's disease. J. Neurol. Neurosurg. Psychiatry 89 (4), 352–357.
Prins, N.D., Scheltens, P., 2015 Mar. White matter hyperintensities, cognitive impairment and dementia: an update. Nat. Rev. Neurol. 11 (3), 157–165.
Racine, A.M., Adluru, N., Alexander, A.L., Christian, B.T., et al., 2014 Feb 19. Associations between white matter microstructure and amyloid burden in preclinical Alzheimer's disease: a multimodal imaging investigation. Neuroimage Clin 4, 604–614.
Roseborough, A., Ramirez, J., Black, S.E., Edwards, J.D., 2017 Oct. Associations between amyloid β and white matter hyperintensities: a systematic review. Alzheimers Dement 13 (10), 1154–1167.
Rotshenker, S., 2011 Aug 30. Wallerian degeneration: the innate-immune response to traumatic nerve injury. J. Neuroinflammation 8, 109.
Schmidt, P., Gaser, C., Arsic, M., Buck, D., et al., 2012 Feb 15. An automated tool for detection of FLAIR-hyperintense white-matter lesions in Multiple Sclerosis. Neuroimage 59 (4), 3774–3783.
Scott, J.A., Braskie, M.N., Tosun, D., Thompson, P.M., et al., 2015 Dec 1. Cerebral amyloid and hypertension are independently associated with white matter lesions in elderly. Front. Aging Neurosci. 7, 221.
Scott, J.A., Braskie, M.N., Tosun, D., Maillard, P., et al., 2016 Dec. Cerebral amyloid is associated with greater white-matter hyperintensity accrual in cognitively normal older adults. Neurobiol. Aging 48, 48–52.
Skoog, I., Kern, S., Zetterberg, H., Östling, S., et al., 2018. Low cerebrospinal fluid Aβ42 and Aβ40 are related to white matter lesions in cognitively normal elderly. J Alzheimers Dis 62 (4), 1877–1886.
Sled, J.G., Zijdenbos, A.P., Evans, A.C., 1998. A nonparametric method for automatic correction of intensity nonuniformity in MRI data. IEEE Trans. Med. Imag. 17, 87–97.
Strain, J.F., Smith, R.X., Beaumont, H., Roe, C.M., et al., 2018 Jul 24. Loss of white matter integrity reflects tau accumulation in Alzheimer disease defined regions. Neurology 91 (4), e313–e318.
Suárez-Calvet, M., Kleinberger, G., Araque Caballero, M.Á., Brendel, M., et al., 2016 May 2. sTREM2 cerebrospinal fluid levels are a potential biomarker for microglia activity in early-stage Alzheimer's disease and associate with neuronal injury markers. EMBO Mol. Med. 8 (5), 466–476.
Sudre, C.H., Cardoso, M.J., Ourselin, S., 2017 May. Longitudinal segmentation of age-related white matter hyperintensities. Med. Image Anal. 38, 50–64.
Tarantini, S., Tran, C.H.T., Gordon, G.R., Ungvari, Z., et al., 2017 Aug. Impaired neurovascular coupling in aging and Alzheimer's disease: contribution of astrocyte dysfunction and endothelial impairment to cognitive decline. Exp. Gerontol. 94, 52–58.
Tosto, G., Zimmerman, M.E., Hamilton, J.L., Carmichael, O.T., et al., 2015 Dec. The effect of white matter hyperintensities on neurodegeneration in mild cognitive impairment. Alzheimers Dement 11 (12), 1510–1519.
Villeneuve, S., Rabinovici, G.D., Cohn-Sheehy, B.I., Madison, C., et al., 2015 Jul. Existing Pittsburgh Compound-B positron emission tomography thresholds are too high: statistical and pathological evaluation. Brain 138 (Pt 7), 2020–2033.
Weaver, N.A., Doeven, T., Barkhof, F., Biesbroek, J.M., et al., 2019 Aug 9. Cerebral amyloid burden is associated with white matter hyperintensity location in specific posterior white matter regions. pii: S0197-4580 Neurobiol. Aging (19), 30279-9.
Yamazaki, Y., Kanekiyo, T., 2017 Sep 13. Blood-brain barrier dysfunction and the pathogenesis of Alzheimer's disease. Int. J. Mol. Sci. 18 (9) pii: E1965.
Zeydan, B., Schwarz, C.G., Lowe, V.J., Reid, R.I., et al., 2019 Mar 3. Investigation of white matter PiB uptake as a marker of white matter integrity. Ann Clin Transl Neurol 6 (4), 678–688.